NANO MICRO small

Cancer Therapy

Adsorption of Multimeric T Cell Antigens on Carbon Nanotubes: Effect on Protein Structure and Antigen-Specific T Cell Stimulation

Tarek R. Fadel, Nan Li, Smith Shah, Michael Look, Lisa D. Pfefferle, Gary L. Haller, Sune Justesen, Corey J. Wilson, and Tarek M. Fahmy**

Carbon nanotubes (CNTs) have shown great potential for applications in biosensing,[1] diagnostics,[2] and drug delivery.[3] Due to their unique physio-chemical properties, they have recently emerged as a promising platform for cell culture applications, enhancing the culture of stem cells,[4] neurons,[5] or others.[6] Several research groups have indeed demonstrated that nanometer-scale topography is an important feature that can enhance cell adhesion, growth, and function.[7] Yet, it has also been shown that nanoscale roughness can affect the amount, structure, and distribution of adsorbed proteins.[8] For instance, it was shown that proteins adsorbed on nanoparticles retained their structure significantly better when adsorbed on smaller versus larger nanoparticles, as the larger surface curvature in smaller nanoparticles reduced the area of interaction with proteins.[9] However, other studies have also indicated that non-covalent association of certain proteins on a biomaterial surface, while having minimal effect on the bulk material structure, significantly altered the structure of adsorbed proteins.[10]

In light of our previous work exploring the effect of functionalized bundled CNTs (^{b}CNTs) on T cell activation,[11] we hypothesized that ^{b}CNTs could be used as a substrate for antigen-specific T cell culture by presenting more physiological protein stimuli such as peptide-loaded major histocompatibility complex class-I (MHC-I), a multimeric protein ubiquitously used for $CD8^{+}$ T cell activation.[12] As previously reported,[11,13] ^{b}CNTs were synthesized from cobalt-incorporated MCM-41, then functionalized to: (1) yield surface defects on the nanotubes through oxidation resulting in a higher surface area, which can then be exploited to measure protein adsorption; and (2) minimize the role of electrostatic interactions between proteins and the ^{b}CNTs surface in aqueous media by reducing carboxylic and carbonyl groups. In this Communication, we measure the effect of functionalized ^{b}CNTs on the structure and function of MHC-I, and propose a simple method for presenting this multimeric T cell stimulus on ^{b}CNTs without affecting the bulk nanotube structure. First, we compare the adsorption behavior of MHC-I on ^{b}CNTs to a wide range of other globular proteins ranging [13–232] kD; we verify that the magnitude of adsorption on ^{b}CNTs strongly correlates with protein molecular weight, and the size of protein hydrophobic core, in agreement with previous work.[14] Second, we assess the effect of adsorption on the secondary structure of MHC-I and show that MHC-I denatures when adsorbed on ^{b}CNTs, in contrast to BSA and neutravidin. Additional controls involving hydrophilic peptide substitution or addition of excess peptide to MHC-I bound on ^{b}CNTs improve protein stability, thus providing insights on the mechanism of denaturation during adsorption. Finally, we explore the presentation of MHC-I on ^{b}CNTs via a linker, and measure its effect on the stimulation of cytotoxic T cells. Cell culture results indicate that adsorption of neutravidin on ^{b}CNTs (labeled ^{N}CNTs) not only proved to be an effective route for presenting MHC-I, but enhanced the magnitude of T cell response as compared to soluble control. In summary, this work confirms the crucial role protein adsorption plays in exploiting the surface of nanomaterials, and shows, for the first time, that CNT-based substrates can be engineered to efficiently present MHC-I for the antigen-specific stimulation of T cells.

Figure 1 describes our initial approach in assessing the impact of ^{b}CNTs on the adsorption of MHC-I. As highlighted in previous work,[11] ^{b}CNTs present a high surface area (1745 m^2/g) amenable for protein adsorption. Characteristics of the surface are described in supplementary Figure S1 and Table S1, which include: measurements of pore size and surface area using nitrogen physisorption (Figures S1A-C), changes in the level of oxygen containing groups by near-edge X-ray adsorption fine structure (NEXAFS) spectroscopy (Figure S1D), and increase in the defect level due to chemical treatment using Raman spectroscopy (Figure S1E). As shown

Dr. T. R. Fadel, Dr. N. Li, S. Shah, Dr. M. Look,
Prof. L. D. Pfefferle, Prof. G. L. Haller,
Dr. C. J. Wilson, Dr. T. M. Fahmy
Departments of Chemical and Biomedical Engineering
Yale University
P.O. Box 208284, New Haven, Connecticut, USA
Fax: (+1) 203 432-0030
E-mail: Corey.Wilson@yale.edu; Tarek.Fahmy@yale.edu
Dr. S. Justesen
Department of Immunobiology and Microbiology
The Panum Institute Blegdamsvej 3b
2200 N, Copenhagen, Denmark

DOI: 10.1002/smll.201201684

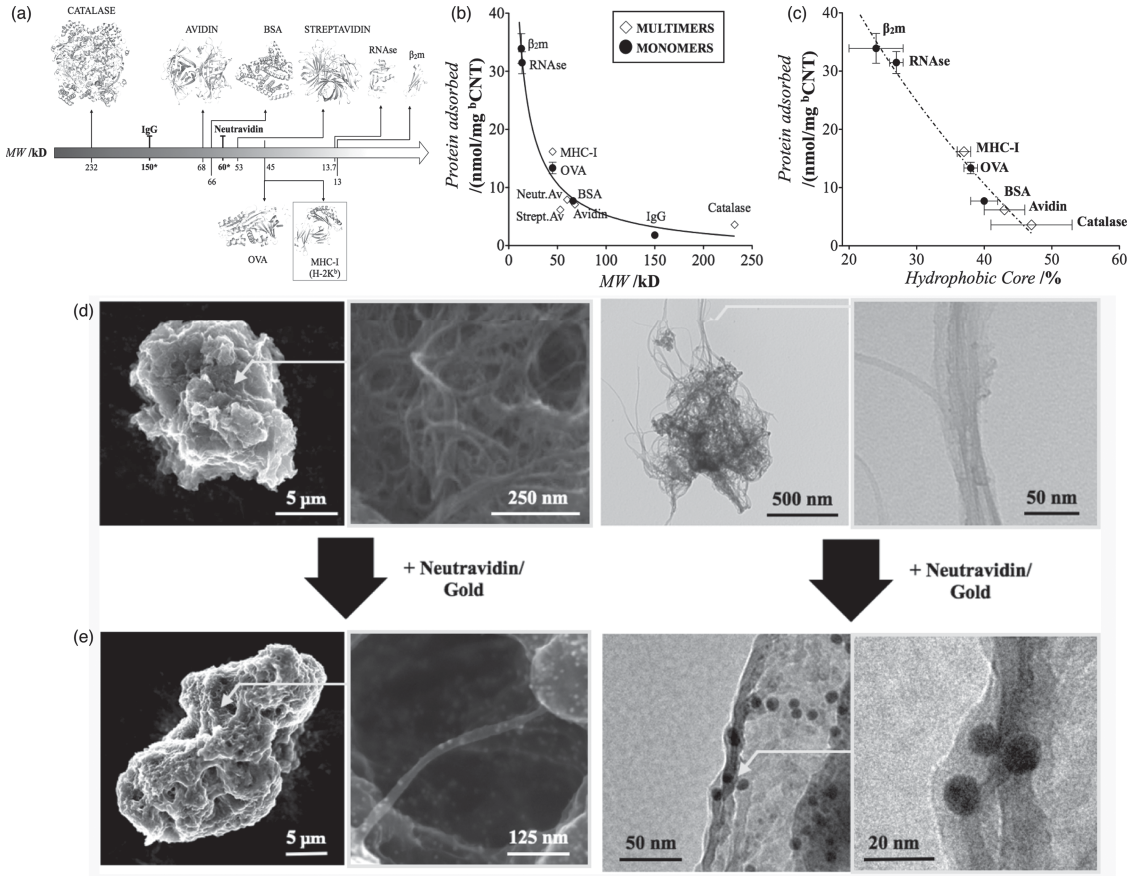

Figure 1. Measurement of protein adsorption on ^{b}CNTs. (A) Crystal structures of proteins ranging [13-232] kD in size; MHC-I complex is highlighted in red. (*) Refers to crystal structures that were currently unavailable. (B) Plot of adsorption values as a function of molecular weight, fitted using a power series model. (C) Plot of adsorption values as a function of size of hydrophobic core (fitted using a power series model). (D) SEM images of ^{b}CNTs before (top) and after (bottom) the adsorption of gold-tagged neutravidin (white dots). (E) TEM images of ^{b}CNTs before (top) and after (bottom) the adsorption of gold-tagged neutravidin (black dots). Data in (B, C) are represented as mean +/–SEM.

in Figure 1A, we chose proteins with various molecular weights, structures, and isoelectric points. To contextualize the effect of functionalized ^{b}CNTs on the adsorption of MHC-I, we measured the variation in amount of bound protein as a function of protein molecular weight (Figure 1B, Table S2), and the percentage of putative hydrophobic core (Figure 1C). We also compared the adsorption of proteins on ^{b}CNTs as a function of molecular weight to activated carbon, another carbon nanomaterial with a similarly high surface area (1762 m^2/g). Figure S2 indicates that protein adsorption occurs at higher magnitude on ^{b}CNTs, in agreement with previously published results.[11] As expected, there is a strong correlation (r^2>0.9) on the amount of protein adsorbed on ^{b}CNTs as a function of molecular weight, ranging between 13 to 232 kD. This occurs despite significant differences in isoelectric points (IP) for certain proteins of similar sizes (for instance: streptavidin IP~5, neutravidin IP~6.3, and avidin IP~10.5). Yet, when measuring the amount of MHC-I complexes adsorbed directly on ^{b}CNTs, we observed that the quantity of protein adsorbed was slightly higher than ovalbumin (OVA), a monomeric protein of similar molecular weight. To investigate this further, we estimated the percentage of putative hydrophobic core (the fraction of the protein that does not come into contact with water) for each protein using a Connolly algorithm.[15] For all of the proteins with solved X-ray crystal structures, we calculated that the percentage of core residues increased with molecular weight, as illustrated by a 2.5 fold increase in percent hydrophobic core for catalase (232 kD) in comparison to a sub-unit of MHC-I, beta-2-microglobulin (β_2m, 13 kD). As expected, we also observed that the magnitude of adsorption for the given proteins on ^{b}CNTs had a strong dependence on the percentage of hydrophobic core with a strong linear correlation for the measured proteins ($r^2 > 0.9$). Furthermore, the results showed that the proportion of hydrophobic core residues in MHC-I was slightly lower than OVA, supporting the difference in measured amounts between the two proteins when adsorbed on ^{b}CNTs. Imaging of ^{b}CNTs at the micro and nano scales revealed the presence of nanotubes aggregating into micron-sized bundles, exhibiting a porous morphology with structural gaps potentially amenable for the adsorption of proteins (Figure 1D, left panel). TEM images of ^{b}CNTs showed the presence of long tubes with a diameter in the nanometer range, lengths in the hundreds of nanometers, and a relatively low density of impurities (Figure 1E, left panel). In order to visualize the assembly of proteins on the surface of ^{b}CNTs, we used

small 2012,
DOI: 10.1002/smll.201201684

NANO MICRO small

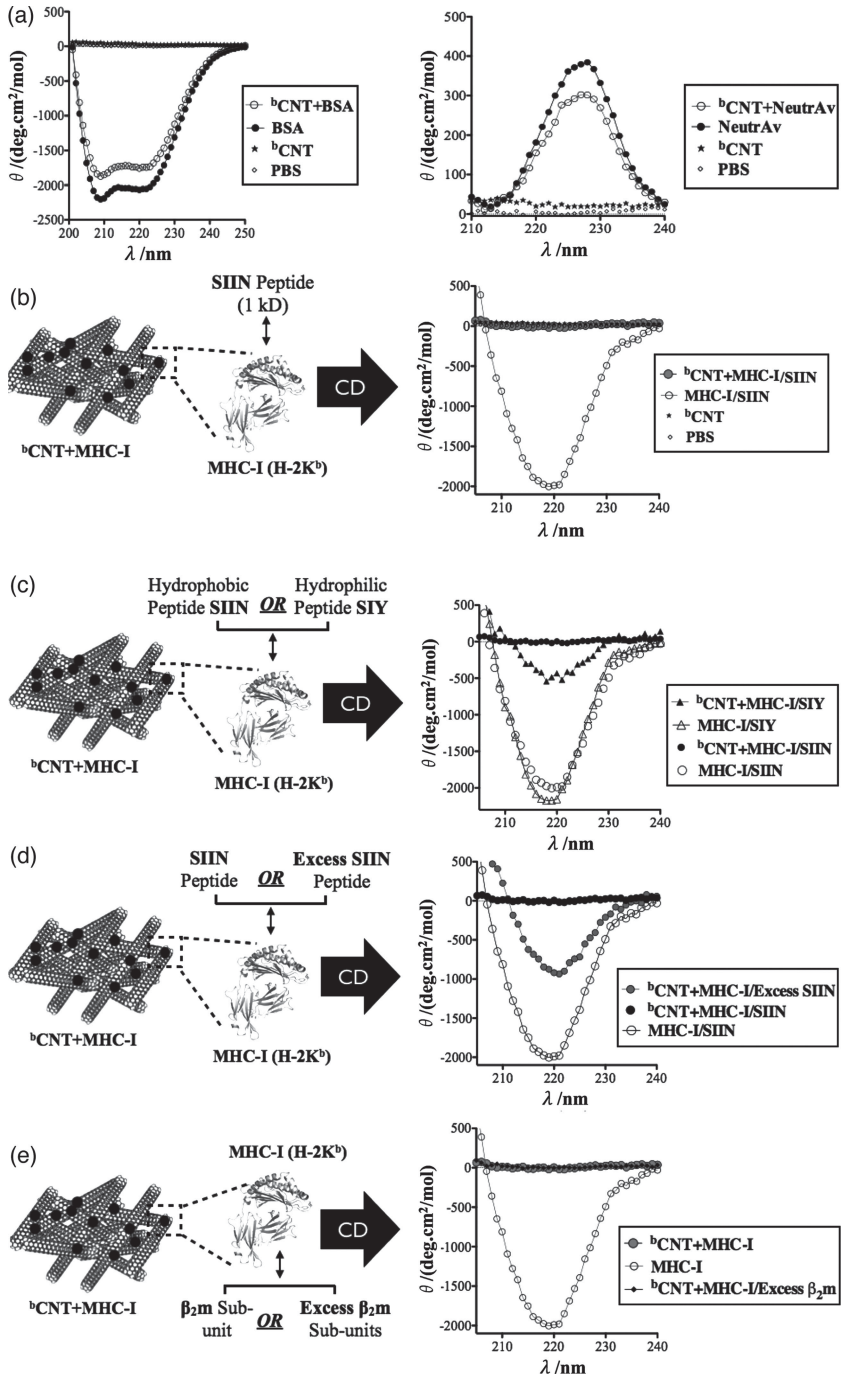

Figure 2. Comparative studies resolving the changes in MHC-I structure as a result of adsorption on ^{b}CNTs. (A) CD spectra of control proteins BSA (left) and neutravidin (right) after adsorption on ^{b}CNTs. (B) Schematic describing the form of MHC-I measured (left, loaded with SIIN peptide) for CD spectroscopy (right) after interaction with ^{b}CNTs. (C) Schematic describing the form of MHC-I measured (left, loaded with SIIN or SIY peptide) for CD spectroscopy (right) after interaction with ^{b}CNTs. (D) Schematic describing the form of MHC-I measured (left, loaded with SIIN or excess SIIN peptide) for CD spectroscopy (right) after interaction with ^{b}CNTs. (E) Schematic describing the form of MHC-I measured (left, loaded with a regular amount of β_2m or excess β_2m) for CD spectroscopy (right) after interaction with ^{b}CNTs.

a model system (neutravidin) tagged with a gold particle of 10 nm in diameter. Electron microscopy images at the micron and nanoscale levels revealed successful adsorption of the protein on the vast nanotube networks (Figure 1D–E, right panels). Processing of these images indicated that neutravidin gold particles adsorbed at a density of 1933 (+/– 431) particles/μm^2, corresponding to a coverage of ~25% of the ^{b}CNT surface.

Far-UV circular dichroism (CD) spectra measurement was conducted to probe the impact of ^{b}CNTs on the structure of adsorbed MHC-I (**Figure 2**). We chose to compare it to two structurally distinct model proteins: BSA (66 kD) and neutravidin (60 kD). BSA is primarily composed of α-helical secondary structure elements, and is a known for its overall stability in physiological conditions. Neutravidin is a (mostly β-sheet) tetrameric protein that is part of the avidin family, known for its strong affinity to biotin, and overall neutral charge in physiological pH. Finally, the MHC-I (composed of α/β structural elements) is a non-covalently associated heterotrimeric complex typically found on the surface of nucleated cells, allowing cytotoxic T cells in the body to discriminate self from non-self. It is formed by a heavy chain (33 kD), the small β_2m subunit, and a peptide typically 8-11 amino acids in length presented in a groove of the heavy chain (in this case SIIN). The stability of this complex relies on non-covalent association of both the SIIN peptide and β_2m, which ultimately facilitates successful T cell receptor recognition and subsequent T cell activation.[12] Initially, each protein was added at an excess concentration (1.25 μM) to saturate the surface of ^{b}CNTs (2-3 fold excess). Concisely, we observed that BSA preserved its characteristic α-helix structure after adsorption, with canonical minima at 208 and 222 nm (Figure 2A, left graph). Though, apparent reductions in BSA molar ellipticity at 222 nm and fluorescence emission at λ_{em} = 340 nm (see Figure S3, left graph) were observed upon adsorption to ^{b}CNTs when compared to BSA alone at the same concentration. This could be attributed to a slight adjustment of adsorbed protein, presumably by the ^{b}CNT surface. A similar effect was observed with neutravidin; namely, characteristic positive cotton effects[16] observed in the 220 to 240 nm range, although at a lower intensity when compared to neutravidin without ^{b}CNTs in solution at the same concentration (Figure 2A and S3, right graphs). Thus, both BSA and neutravidin preserved most of their secondary structure on ^{b}CNTs after adsorption.

Adsorption of MHC-I loaded with SIIN (MHC-I/SIIN) on ^{b}CNTs produced the most drastic case of protein denaturation in comparison to BSA and neutravidin

DOI: 10.1002/smll.201201684

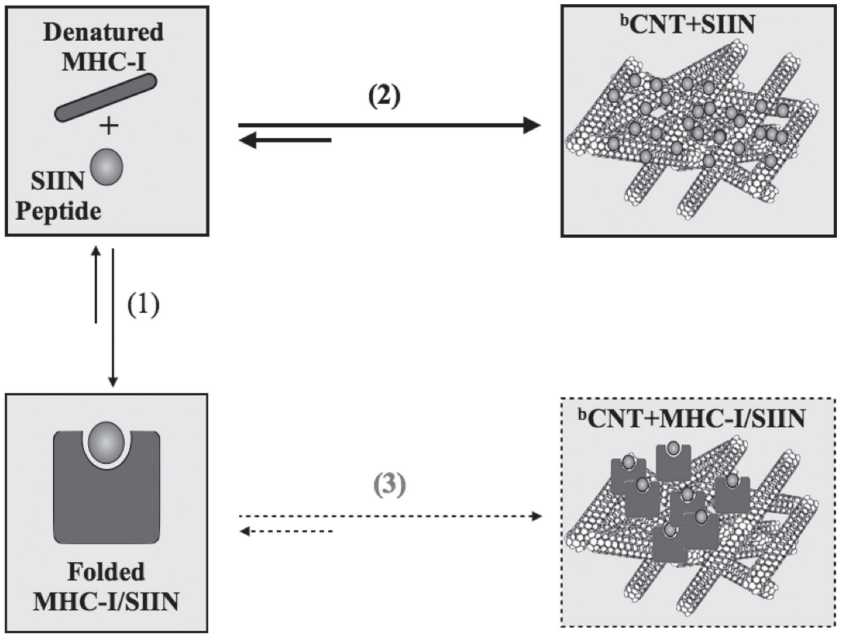

LEGEND:
(1) Binding of SIIN peptide to MHC-I
(2) Denaturation of MHC-I through binding of SIIN to ^{b}CNT
(3) Adsorption of folded MHC-I/SIIN to ^{b}CNT

Figure 3. Schematic illustrating the mechanism of MHC-I denaturation on ^{b}CNTs. This mechanism is described by two competitive binding events, both driven by hydrophobic interactions: the binding of the peptide to MHC-I shown in event (1), which stabilizes the assembly, and the binding of SIIN directly to ^{b}CNTs (2). The binding event (2), shown in bold, predominates in the presence of ^{b}CNTs, while the adsorption of stable MHC-I on ^{b}CNTs, which is given by (3) and shown in dashed lines, is unlikely due to the denaturation of MHC-I triggered by event (2). Interaction of β_2m with MHC-I was not included in this schematic since it was not considered a major factor in the mechanism of MHC-I denaturation on ^{b}CNTs.

(Figure 2B). The molar ellipticity for MHC-I/SIIN indeed changes significantly upon adsorption on ^{b}CNTs when compared to soluble MHC-I/SIIN. Considering the non-covalent and allosteric interactions stabilizing this heterotrimer,[17] we hypothesized that adsorption of MHC-I on ^{b}CNTs would disturb this assembly by preferentially binding to hydrophobic components, thus compromising the structural integrity of the protein assembly. Adsorption isotherms of MHC-I and its subcomponents on ^{b}CNTs indicate that such interaction could occur especially when considering the hydrophobic nature of the SIIN peptide. Results in Figures S4 show that the adsorption isotherms for each component saturate at ~3800 nmol of SIIN (left panel), ~16 nmol of MHC-I (middle panel), and ~34 nmol of β_2m (right panel) per mg of ^{b}CNT. In this case, the magnitude of SIIN bound on ^{b}CNT is more than 100-fold the magnitude of β_2m, despite the peptide having a molecular weight 13-times smaller than β_2m.

To assess how each component within the heterotrimer affects the structure of MHC-I on ^{b}CNTs, we compared the putative stability of MHC-I loaded with a more hydrophilic peptide SIYRYYGL (SIY) as shown in Figure 2C. The results indicate that MHC-I/SIY adsorption on ^{b}CNTs had a diminished impact on the overall secondary structure, relative to MHC-I loaded with SIIN. Next, we investigated the effect of adding excess SIIN peptide or the β_2m subunit exogenously on improving the stability of MHC-I/SIIN adsorbed on ^{b}CNTs. We added 10 μM of SIIN peptide along with the multimer (i.e., ^{b}CNT+MHC-I/Excess SIIN), and compared the CD spectra of the complex in the presence of excess peptide to soluble MHC-I/SIIN and ^{b}CNT+MHC-I/SIIN (Figure 2D). The addition of excess peptide did indeed preserve a significant fraction of the MHC-I/SIIN secondary structure. In contrast, addition of a nine-fold excess amount of β_2m along with the multimer did not have an impact on the secondary structure of adsorbed MHC-I on ^{b}CNTs (Figure 2E). Similar trends were observed by way of intrinsic tryptophan emissions using the same protein-peptide complexes, supporting a strong correlation between global and local events upon adsorption (refer to Figure S5). Ultimately, these results indicate so far that the process of adsorption on ^{b}CNTs can have drastic effects on the secondary structure of MHC-I, as the biomaterial also binds the endogenous peptide SIIN typically associated with the MHC complex. A mechanism for the denaturation of the major MHC-I on ^{b}CNTs is proposed in **Figure 3**. The denaturation of MHC-I on ^{b}CNTs can be described by two competitive binding events both driven by hydrophobic interactions: (1) the binding of SIIN to MHC-I, which stabilizes the assembly, and (2) SIIN binding directly to ^{b}CNTs due to the hydrophobic nature of the biomaterial. Since loading of SIIN to a MHC-I molecule include the interplay of hydrophobic forces, which govern binding and anchoring of the peptide within the MHC cleft, any competing hydrophobic interactions will significantly affect the structural integrity of the protein, thus making the adsorption of stable MHC-I on ^{b}CNTs unlikely.

As a proof of concept, we explored a simple method to present the physiological complex MHC-I on ^{b}CNTs for the culture of cytotoxic T cells (**Figure 4**). Consistent with earlier figures (Figure 1–Figure 3), and based on the results from Figure S6 in which we characterized other methods to present biotinylated MHC-I on ^{b}CNTs, we chose to adsorb neutravidin on ^{b}CNTs (labeled ^{N}CNTs) to bind biotinylated MHC-I/SIIN. Successful adsorption of neutravidin on ^{b}CNTs allows for the stable presentation of biotinylated stimulus, and takes advantage of the unique nanoscale surface properties of carbon nanotube substrates for protein adsorption and cell interaction. Immunofluorescence results reveal the accessibility of the MHC-I antigenic epitope for binding to an antibody specific to stable MHC-I/SIIN, 25-D1.16

DOI: 10.1002/smll.201201684

NANO MICRO small

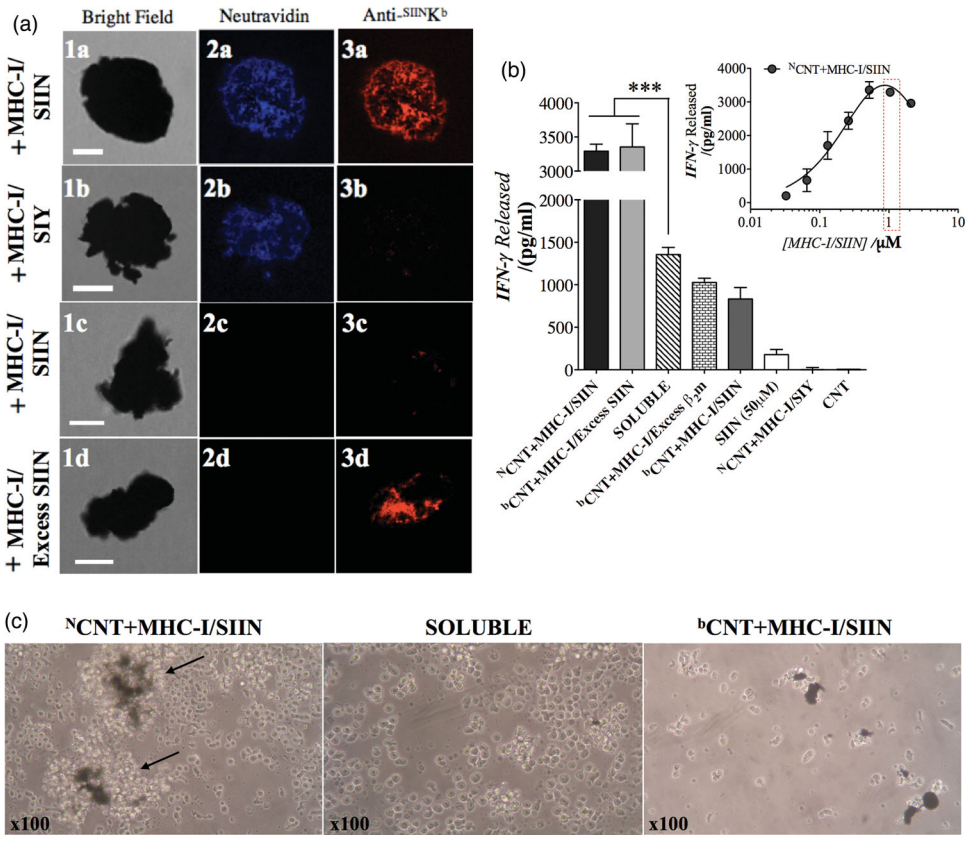

Figure 4. Enhancing antigen-specific T cell response using ^{N}CNTs. (A) Confocal fluorescence images of ^{b}CNT functionalized with neutravidin DL405, presenting either biotinylated MHC-I/SIIN or MHC-I/SIY complexes, and stained with anti-MHC-I/SIIN (25-D1.16 antibody tagged with PE). Top two rows are images of neutravidin bound ^{b}CNT in brightfield (1a, 1b), in the DL405 channel (2a, 2b) and in the PE channel (3a, 3b). Bottom two rows are images of ^{b}CNT directly adsorbing MHC-I/SIIN or MHC-I/SIY complexes in brightfield (1c, 1d), in the DL405 channel (2c, 2d) and in the PE channel (3c, 3d). Each scale bar represents 10 μm. These images are representative of at least 5 independent experiments. (B) IFN-γ response from CD8+ T cells interacting with various CNT platforms in comparison to control; inset: IFN-γ levels from CD8+ T cells interacting with ^{N}CNT+MHC-I/SIIN at various concentrations of biotinylated MHC-I/SIIN; selected concentration shown in red. Data are represented as mean +/−SD. (C) Phase-contrast microscopy images of T cells interacting with ^{N}CNT+MHC-I/SIIN in comparison to control (day 3); black arrows point towards lymphoblast formation.

(Figure 4A). Results shown in the DL405 and PE channels confirm the presence of neutravidin adsorbed on ^{b}CNTs to form ^{N}CNTs (images 2a and 2b), as well as a stable and well-ordered biotinylated MHC-I/SIIN complex conjugated to ^{N}CNTs (image 3a). The 25-D1.16 monoclonal antibody reacts specifically with the ovalbumin-derived peptide SIIN bound to the given MHC-I, but not an MHC-I bound with an analog peptide such as SIY.[18] Accordingly, we immobilized biotinylated MHC-I loaded with the peptide SIY on ^{N}CNT, as a control for retained specificity upon conjugation; as expected, we observed a minimal response from ^{N}CNT+MHC-I/SIY (image 3b). Binding of MHC-I/SIIN directly to ^{b}CNT also resulted in minimal staining with 25-D1.16 (image 3c) due to the significant loss of secondary structure of the complex (Figure 2C), whereas addition of excess SIIN peptide (10 μM) produced a positive stain using 25-D1.16 (image 3d). Next, we monitored the incubation of cytotoxic T cells with ^{N}CNT+MHC-I/SIIN over a period of 3 days to assess the magnitude of cell response. We used in this case cells isolated from an OT-1 transgenic mouse, which express a T cell receptor specific for the SIIN peptide presented in the context of MHC-I, but does not recognize MHC-I loaded with a different peptides (i.e. SIY). Figure 4B shows the response from stimulated T cells by measuring IFN-γ, a pro-inflammatory cytokine, 3 days after incubation with controls and ^{N}CNTs at an optimal MHC-I/SIIN concentration of ~1.1 μM (Figure 4B, inset). ^{N}CNT+MHC-I/SIIN enhanced T cell response with IFN-γ values reaching close to 3500 pg/mL, three-fold the level reached by "Soluble" control (biotinylated MHC-I bound to neutravidin at similar amounts), while MHC-I directly adsorbed on ^{b}CNT triggered a significantly lower T cell response with IFN-γ values below 1000 pg/mL. Note that this enhancement in T cell response in comparison to soluble controls did not only apply to ^{N}CNT+MHC-I/SIIN, but also to avidin adsorbed ^{b}CNTs presenting MHC-I (^{A}CNT+MHC-I/SIIN), and streptavidin bound ^{b}CNTs presenting MHC-I (^{S}CNT+MHC-I/SIIN) as given in Figure S6.

Addition of excess SIIN peptide (^{b}CNT+MHC-I/Excess SIIN) activated T cells to a level similar to ^{N}CNT+MHC-I/SIIN, in agreement with the results in Figure 2D. As expected, addition of excess β_2m along with the multimer (^{b}CNT+MHC-I/Excess β_2m) did not have an impact on the

DOI: 10.1002/smll.201201684

level of T cell response when compared to ^{b}CNT+MHC-I/SIIN, in agreement with the mechanism proposed in Figure 3. Finally, ^{N}CNT+MHC-I/SIY, ^{b}CNT, and soluble peptide triggered no response. Imaging of T cells on ^{N}CNT+MHC-I/SIIN three days after incubation showed the formation of several large lymphoblasts (Figure 4C, left panel as indicated by black arrows) at higher extent than soluble controls and CNT+MHC-I/SIIN (Figure 4C, panels b and c, respectively). Together, these results show for the first time that a complex multimeric protein can be stabilized on functionalized bulk CNTs to enhance the culture of antigen-specific T cells.

In summary, we evaluated the stability and function of a physiological multimeric protein, MHC-I, on ^{b}CNTs for applications related to antigen-specific T cell stimulation. We measured the interaction of MHC-I with ^{b}CNTs by comparing its adsorption on the biomaterial to a wide range of other proteins with molecular weights between 13 and 232 kD, and verified the importance of hydrophobic interactions during MHC-I adsorption. Spectra measurements of MHC-I loaded with various peptide formulations confirmed that this process of adsorption significantly denatured MHC-I/SIIN on ^{b}CNTs, while other controls such neutravidin or BSA showed remarkable tolerance to binding the biomaterial. We consequently proposed a simple method to present the physiological T cell stimulus by exploiting the stability of neutravidin on ^{b}CNTs, and used neutravidin-biotin chemistry for presentation of biotinylated MHC-I/SIIN on ^{N}CNTs. Our results indicate that our method enhanced antigen-specific T cell response more than three-fold when compared to soluble control in similar conditions. Ultimately, this work provides an insight into the use of non-covalent chemistry and adaptor proteins to present complex stimuli on carbon nanotube substrates. It also points the potential of bundled CNTs in T cell culture applications related to immunotherapy.

Experimental Section

Carbon Nanotubes: ^{b}CNTs were synthesized from cobalt-incorporated MCM-41 (Co-MCM-41) to obtain bulk low-defect-density nanotubes. The nanotubes were purified using a mild, four-step treatment procedure consisting of NaOH reflux, HCl wash, and oxidation by molecular oxygen (4 mol%). Samples were washed twice in sodium hydroxide for 1 h, followed by subsequent filtration using a PTFE filter. A second cleaning step was carried out using hydrochloric acid at 60 °C overnight. To remove amorphous carbon particulates, samples were heated in oxygen stream (4 mol%) in a quartz reactor at 300 °C followed by repeated HCl washing, filtration, and drying steps. Functionalized carbon nanotubes were produced by stirring samples in HNO_3 (3 M) at 70 °C for 1 h, followed by filtration using a 5 μm pore size PTFE membrane and drying at 45 °C overnight. Samples were then reduced by the addition of $LiBH_4$ solution in THF and sonication for 1.5 h.

Protein Adsorption and Stability Studies: Protein samples (concentrations ranging from 100-300 μg/mL) were serially diluted in PBS. ^{b}CNT suspension in PBS was sonicated for 10 min to obtain uniform dispersion then added at an equal volume to each of the protein solution. The mixture was allowed to mix in a rotary shaker at 4 °C overnight. ^{b}CNT-protein mixtures were then centrifuged in a micro-centrifuge at 15 000 rpm for 20 min. The supernatant (free of CNT particles) was removed, and analyzed for protein content using the bicinchoninic acid (BCA) assay. For the measurement of SIIN peptide adsorption on ^{b}CNTs, we analyzed the supernatants using the o-phthalaldehyde (OPA) assay. The amount of protein adsorbed onto ^{b}CNT was deduced from a simple mass balance based on the difference in protein concentration before and after ^{b}CNT adsorption. Maximal adsorption (nmol adsorbed per mg of ^{b}CNT) was derived from a one-phase association model of each isotherm and calculated by dividing the plateau adsorption value by the concentration of ^{b}CNTs used in the study.

A solvent-accessible surface was computed around the backbone and side-chain structures for each model protein, using the Connolly algorithm. The Connolly surface was generated by rolling a spherical water probe with an 8 Å radius along the van der Waals spheres of the outer (accessible) atoms of a given PDB coordinate set: β_2m (1LSD), RNAse (2G8Q), ovalbumin (1OVA), MHC-I (1VAC), streptavidin (1STP), BSA (3V03), avidin (1RAV), catalase (3NWL). A given three-dimensional coordinate set was first reduced (in silico) to model-in non-resolvable hydrogen atoms, using the Richardson's MolProbity program.[19] Next, each structure was energy minimized using a conjugate gradient method (50 steps) to relax the structure. Finally, Connolly dots are added to form a surface tangent to both the probe and putative protein surface, in turn residues were partitioned into two classes solvent, exposed and core. The ratio of core to total observed residues gives the% hydrophobic core.% Error was determined by the ratio of observed residues relative to the reported full-length primary structure.

Circular Dichroism CD Spectroscopy: Protein/ Protein-CNT CD was monitored by far-UV CD at 190–240 nm using an Applied Photophysics (Leatherhead, UK) spectrometer. Far-UV CD measurements report on the global secondary structure of a given protein. Sample preparation is as follows, ^{b}CNT were diluted (50 μg/mL) in a protein solution (1.25 μM) in PBS and tumbled overnight at 4 °C. Spectroscopic handles were collected with 4 nm bandwidth, and a 1 s average per nm step. The resulting millidegrees were normalized to molar ellipticity using following the equation:

$$([\theta] = \frac{MRW.[\theta]Obs}{l.C}) \quad (1)$$

where mean residue molecular weight *MRW* is the ratio of molecular weight (g/mol) to (number of amino acids-1), $[\theta]_{obs}$ is the ellipticity measured in millidegrees, path length l is 10 mm, and concentration C is in mg/mL.

Imaging of b*CNT-Protein Interaction*: HR-SEM images were obtained on a Hitachi SU-70 high-resolution microscope (Norcross, Georgia) with an accelerating voltage of 10 kV. For imaging of protein adsorption, neutravidin (50 μg/mL) tagged with nanogold particles (10 nm in diameter) was added to ^{b}CNT (50 μg/mL) in PBS. The mixture was tumbled at 4 °C overnight, washed twice in water and allowed to air dry before imaging.

TEM images were obtained using a Philips Tecnai F12 TEM instrument. Pre-weighed ^{b}CNT (1 mg) was mixed in ethanol (10 ml, ACS/USP grade), and dispersed by ultra-sonication. A droplet of the CNT/ethanol suspension was then applied on a holey coated copper TEM grid before air-drying. For imaging of protein adsorption, neutravidin tagged with nanogold particles (10 nm in diameter) was added to pre-sonicated ^{b}CNT (50 μg/mL) in PBS. The

small 2012,
DOI: 10.1002/smll.201201684

mixture was tumbled at 4 °C overnight, washed twice and diluted (5 μg/mL) in water, then applied on a holey coated copper TEM grid before drying under vacuum.

Antigen-Specific T Cell Stimulation Studies: OT-1 mice (in which CD8+ T cells express a transgenic TCR specific for the SIIN peptide of ovalbumin presented on H-2K^b) were bred, maintained and screened in the Malone Engineering Center at Yale University. Splenocytes were isolated from the spleen of OT-1 mice (aged 6–8 weeks) after depletion of erythrocytes by hypotonic lysis. CD8+ T cells were isolated using the Stem Cell CD8$^+$ negative selection kit. CD8$^+$ T cells were resuspended in cell media, composed of RPMI 1640 supplemented with FBS (10%), L-glutamine (1%), HEPES buffer (1%), non-essential amino acids, 2-ME (0.1%), penicillin (2%), and stored at 4 °C before use. ^{b}CNTs (50 μg/mL) were sonicated at in PBS using a Branson B300 ultrasonicator (Danbury, CT) for 5 min. The nanotube solution was then suspended in a solution of neutravidin (0.8 μM) in PBS, incubated overnight at 4 °C. Biotinylated H-2K^b (MHC-I loaded with SIINFEKL peptides or MHC/SIIN) was added along with αCD28 (total concentration 2.1 μM) to the ^{N}CNT suspension and allowed to mix for 1 hr at room temperature. The mixture was then diluted in cell media (1:5) then added to an equal volume of CD8$^+$ T cells (5×10^5 cells/mL). A sandwich ELISA protocol was used to measure mouse IFN-γ production

Supporting Information

Supporting Information is available from the Wiley Online Library or from the author.

Acknowledgements

We acknowledge Professor Paul Van Tassel, Aimon Iftikhar, Changchang Liu, Fang Fang, Ragy Ragheb, Mark Schwab, and Doyle P. Bean for their help in this study. This work was supported by the NSF Career Award (0747577) to T.M.F

[1] a) F. Balavoine, P. Schultz, C. Richard, V. Mallouh, T. W. Ebbesen, C. Mioskowski, *Angew. Chem. Int. Ed.* **1999**, *38*, 1912–1915; b) P. W. Barone, S. Baik, D. A. Heller, M. S. Strano, *Nat. Mater.* **2005**, *4*, 86–92.

[2] a) R. Singhal, Z. Orynbayeva, R. V. Kalyana Sundaram, J. J. Niu, S. Bhattacharyya, E. A. Vitol, M. G. Schrlau, E. S. Papazoglou, G. Friedman, Y. Gogotsi, *Nat. Nanotechnol.* **2011**, *6*, 57–64; b) S. Y. Hong, G. Tobias, K. T. Al-Jamal, B. Ballesteros, H. Ali-Boucetta, S. Lozano-Perez, P. D. Nellist, R. B. Sim, C. Finucane, S. J. Mather, M. L. Green, K. Kostarelos, B. G. Davis, *Nat. Mater.* **2010**, *9*, 485–490.

[3] a) W. Wu, R. Li, X. Bian, Z. Zhu, D. Ding, X. Li, Z. Jia, X. Jiang, Y. Hu, *ACS Nano* **2009**, *3*, 2740–2750; b) H. Huang, Q. Yuan, J. S. Shah, R. D. Misra, *Adv. Drug Deliv. Rev.* **2011**, *63*, 1332–1339.

[4] a) Y. J. Huang, H. C. Wu, N. H. Tai, T. W. Wang, *Small* **2012**; b) T. R. Nayak, L. Jian, L. C. Phua, H. K. Ho, Y. P. Ren, G. Pastorin, *ACS Nano* **2010**, *4*, 7717–7725.

[5] E. B. Malarkey, K. A. Fisher, E. Bekyarova, W. Liu, R. C. Haddon, V. Parpura, *Nano Lett.* **2009**, *9*, 264–268.

[6] L. P. Zanello, B. Zhao, H. Hu, R. C. Haddon, *Nano Lett.* **2006**, *6*, 562–567.

[7] a) C. J. Bettinger, R. Langer, J. T. Borenstein, *Angew. Chem. Int. Ed.* **2009**, *48*, 5406–5415; b) V. Brunetti, G. Maiorano, L. Rizzello, B. Sorce, S. Sabella, R. Cingolani, P. P. Pompa, *Proc. Natl. Acad. Sci. USA* **2010**, *107*, 6264–6269; c) R. J. McMurray, N. Gadegaard, P. M. Tsimbouri, K. V. Burgess, L. E. McNamara, R. Tare, K. Murawski, E. Kingham, R. O. C. Oreffo, M. J. Dalby, *Nat. Mater.* **2011**, *10*, 637–644; d) M. M. Stevens, J. H. George, *Science* **2005**, *310*, 1135–1138.

[8] a) T. R. Fadel, M. Look, P. A. Staffier, G. L. Haller, L. D. Pfefferle, T. M. Fahmy, *Langmuir* **2010**, *26*, 5645–5654; b) P. Roach, D. Farrar, C. C. Perry, *J. Am. Chem. Soc.* **2006**, *128*, 3939–3945; c) T. F. Keller, J. Schonfelder, J. Reichert, N. Tuccitto, A. Licciardello, G. M. L. Messina, G. Marletta, K. D. Jandt, *ACS Nano* **2011**, *5*, 3120–3131.

[9] a) M. Lundqvist, I. Sethson, B. H. Jonsson, *Langmuir* **2004**, *20*, 10639–10647; b) A. A. Vertegel, R. W. Siegel, J. S. Dordick, *Langmuir* **2004**, *20*, 6800–6807.

[10] a) J. T. Cang-Rong, G. Pastorin, *Nanotechnology* **2009**, *20*, 255102; b) S. S. Karajanagi, A. A. Vertegel, R. S. Kane, J. S. Dordick, *Langmuir* **2004**, *20*, 11594–11599; c) J. W. Shen, T. Wu, Q. Wang, Y. Kang, *Biomaterials* **2008**, *29*, 3847–3855.

[11] T. R. Fadel, E. R. Steenblock, E. Stern, N. Li, X. Wang, G. L. Haller, L. D. Pfefferle, T. M. Fahmy, *Nano Lett.* **2008**, *8*, 2070–2076.

[12] K. Murphy, P. Travers, M. Walport, *Janeway's Immunobiology*, 7th ed., Garland Science, New York (NY) **2007**.

[13] Y. Chen, L. Wei, B. Wang, S. Lim, D. Ciaparu, M. Zheng, J. Chen, C. Zoican, Y. Yang, G. L. Haller, L. D. Pfefferle, *ACS Nano* **2007**, 1, 327–336.

[14] a) P. Parhi, A. Golas, N. Barnthip, H. Noh, E. A. Vogler, *Biomaterials* **2009**, *30*, 6814–6824; b) E. A. Vogler, *Biomaterials* **2012**, *33*, 1201–1237.

[15] M. L. Connolly, *J. Appl. Crystallogr.* **1983**, *16*, 548–558.

[16] N. M. Green, M. D. Melamed, *Biochem. J.* **1966**, *100*, 614–621.

[17] D. M. Gakamsky, L. F. Boyd, D. H. Margulies, D. M. Davis, J. L. Strominger, I. Pecht, *Biochemistry* **1999**, *38*, 12165–12173.

[18] A. Porgador, J. W. Yewdell, Y. Deng, J. R. Bennink, R. N. Germain, *Immunity* **1997**, *6*, 715–726.

[19] V. B. Chen, W. B. Arendall, 3rd, J. J. Headd, D. A. Keedy, R. M. Immormino, G. J. Kapral, L. W. Murray, J. S. Richardson, D. C. Richardson, *Acta Crystallogr. D* **2010**, *66*, 12–21.

Received: July 15, 2012
Revised: August 21, 2012
Published online: